Applied Catalysis B: Environmental 313 (2022) 121449

Contents lists available at ScienceDirect

Applied Catalysis B: Environmental

journal homepage: www.elsevier.com/locate/apcatb

Bidentate ligand modification strategy on supported Ni nanoparticles for photocatalytic selective hydrogenation of alkynes

Jie Wang [a,e,1], Mengxia Wang [d,1], Xincheng Li [a,e,1], Xianmo Gu [a], Peng Kong [a], Ruiyi Wang [a,*], Xuebin Ke [c,*], Guangtao Yu [b,f,**], Zhanfeng Zheng [a,e,***]

[a] State Key Laboratory of Coal Conversion, Institute of Coal Chemistry, Taiyuan 030001, China
[b] Engineering Research Center of Industrial Biocatalysis, Fujian Province University, Fujian Provincial Key Laboratory of Advanced Materials Oriented Chemical Engineering, College of Chemistry and Materials Science, Fujian Normal University, Fuzhou 350007, China
[c] Department of Chemical Engineering, University of Hull, HU6 7RX, United Kingdom
[d] Laboratory of Theoretical and Computational Chemistry, Institute of Theoretical Chemistry Jilin University, Changchun 130023, China
[e] Center of Materials Science and Optoelectronics Engineering, University of Chinese Academy of Sciences, Beijing 100049, China
[f] Fujian Provincial Key Laboratory of Theoretical and Computational Chemistry, Xiamen University, Xiamen 361005, China

ARTICLE INFO

Keywords:
Ni nanoparticles
LSPR
Surface l-lysine
Phenylacetylene hydrogenation
High selectivity and stability

ABSTRACT

The design of selective and stable non-precious metal catalysts for hydrogenation of alkyne is highly desirable. In this study, L-lysine modification strategy is applied to support Ni nanoparticles, which greatly improves the stability and photocatalytic performance in the hydrogenation of phenylacetylene to styrene. The robust stability is attributed to that both amino and carboxyl groups of L-lysine can function simultaneously as the anchor, much stronger than a single group, to strongly interact with metallic Ni via N and O coordination. The high selectivity to styrene is due to that L-lysine modification results in a larger adsorption energy difference between styrene and phenylacetylene on the surface of Ni, therefore phenylacetylene is preferentially adsorbed on Ni surface. This protocol shows that the modulation of interaction between ligands and Ni is favorable to design stable, active and selective catalysts for hydrogenation of alkynes.

1. Introduction

The selective hydrogenation of alkyne to olefin is an important reaction in industry due to its application in pharmaceuticals, agrochemicals, fragrances, polymerization, olefin metathesis reactions and removal of trace alkyne impurities in olefin polymerization industry [1–6]. It is still a great challenge to develop effective catalysts with high catalytic activity and olefin selectivity [7,8]. At present, although Pd and Pt-based catalysts are the most promising ones which show obvious advantages of high olefin selectivity [9–11], the limited resources and high cost limit their practical applications to some extent. Hence, the development of non-precious metal catalysts like earth abundant Ni provides a low-cost solution for selective hydrogenation of alkyne to olefin.

Ni-based catalysts are widely used in the hydrogenation of alkynes due to its high hydrogenation activity, but still suffer from low olefin selectivity [12–19]. A major reason for low olefin selectivity is the strong adsorption capacity of olefins on the surface of Ni. Strategies including alloying, incorporation of *p*-block elements into interstitial sites of Ni and selective coordination with some amino compounds have been attempted [20–24]. For example, the NiGa intermetallic catalysts with completely isolated Ni sites exhibit high ethylene selectivity, which is ascribed to the preferential acetylene adsorption and enhanced ethylene desorption on the surface of Ni sites [21]. Over-hydrogenation of alkynes can also be suppressed by nickel nitride (Ni_3N) via weak interaction between the alkene product and the Ni_3N active sites [24]. Amino compounds have been used as additives in the phenylacetylene hydrogenation reaction system, which can coordinate with Ni-based catalysts

* Corresponding authors.
** Corresponding author at: Engineering Research Center of Industrial Biocatalysis, Fujian Province University, Fujian Provincial Key Laboratory of Advanced Materials Oriented Chemical Engineering, College of Chemistry and Materials Science, Fujian Normal University, Fuzhou 350007, China.
*** Corresponding author at: State Key Laboratory of Coal Conversion, Institute of Coal Chemistry, Taiyuan 030001, China.
E-mail addresses: wangruiyi@sxicc.ac.cn (R. Wang), x.ke@hull.ac.uk (X. Ke), yugt@fjnu.edu.cn (G. Yu), zfzheng@sxicc.ac.cn (Z. Zheng).
[1] These authors contributed equally.

https://doi.org/10.1016/j.apcatb.2022.121449
Received 28 January 2022; Received in revised form 22 April 2022; Accepted 23 April 2022
Available online 26 April 2022

to weaken adsorption of olefins to regulate the hydrogenation of alkynes to olefins [25–27]. It is revealed that the additive *n*-butyl amine with single amino group can increase the alkene selectivity over Ni_1Fe_3 catalyst while facing the difficulty of products separation [27]. Meanwhile, poor stability is also shown over Ni nanoparticles (NPs) modified by imidazolium-amidinate ligands to modulate alkene selectivity [26]. As a consequence, the interaction between single amino compounds and the Ni NPs should be enhanced to fulfill the need of development of an inexpensive, stable, and higher selective Ni-based catalyst in industry and academia.

Recently, it is reported that photoexcited electrons of Ni NPs, due to localized surface plasmon resonance (LSPR) effect under visible light irradiation, can promote catalytic activity and make the reactions proceed at relatively low temperatures [28,29]. Therefore, it is very attractive to drive hydrogenation reaction with solar energy in view of the gradual depletion of fossil resources. This provides a possibility that the activity for phenylacetylene hydrogenation can also be promoted by the LSPR effect of Ni NPs.

Herein, we design an L-lysine (with bidentate ligand, both carboxy and amino groups) modified photocatalyst, i.e. L-lysine modified Ni/Nb_2O_5 (L-lysine/Ni/Nb_2O_5), for photocatalytic hydrogenation of phenylacetylene. Here, Nb_2O_5, a wide band gap semiconductor (~3.2 eV) and irresponsive for visible light ($\geq$ 420 nm) [30], is beneficial to study the photocatalytic properties promoted by the LSPR effect of metal Ni NPs under visible light irradiation. L-lysine/Ni/Nb_2O_5 can achieve high conversion of phenylacetylene while maintaining high styrene selectivity and can be used for several times with a good stability. The high selectivity to styrene is due to that L-lysine modification results in a larger adsorption energy difference between styrene and phenylacetylene on the surface of Ni. The improved stability of Ni-based catalysts is attributed to the strong co-interaction between bidentate ligand of L-lysine and Ni/Nb_2O_5.

2. Experimental section

2.1. Chemicals

Hydrochloric acid (HCl, 36–38%), niobium pentoxide (Nb_2O_5, $\geq$99.99%), nickel nitrate hexahydrate ($Ni(NO_3)_2.6\ H_2O$), L-lysine, D-lysine, DL-lysine and styrene were purchased from Sinopharm Chemical Reagent Co. Ltd and used without further purification. Sodium hydroxide (NaOH) was purchased from Tianjin Kemiou Chemical Reagent Co. Ltd. Phenylacetylene was purchased from Aladdin.

2.2. Preparation of Ni-niobate (10 wt%Ni)

0.3 g of H-niobate, which was obtained according to previous report [30–32], and 0.1651 g of $Ni(NO_3)_2.6\ H_2O$ were put into 50 mL of 0.04 M L-lysine aqueous solution. The obtained mixture was placed in a teflon-lined, sealed with stainless-steel vessel with an inner volume of 100 mL, and then maintained for 24 h at 180 °C. The product was washed with ultrapure water and dried at 80 °C for 12 h and labeled as Ni-niobate.

2.3. Preparation of Ni/Nb_2O_5, NiO/Ni/Nb_2O_5 and NiO/Nb_2O_5

For a typical synthesis of 10 wt%Ni/Nb_2O_5, the prepared Ni-niobate was reduced at 600 °C for 3 h by H_2 (10 mL min^{-1}) in tube furnace to obtain final Ni/Nb_2O_5. Other loadings of Ni NPs were also prepared by the similar method with addition of different amounts of $Ni(NO_3)_2.6\ H_2O$ in the preparation of Ni-niobate. To obtain NiO/Ni/Nb_2O_5 or NiO/Nb_2O_5 having identical Ni loadings with 10 wt%Ni/Nb_2O_5, above 10 wt%Ni/Nb_2O_5 was annealed in Air for 2 h at 200 and 500 °C, respectively. Unless otherwise specified, the Ni/Nb_2O_5 below represents 10 wt%Ni/Nb_2O_5.

2.4. Preparation of L-lysine/Ni/Nb_2O_5

The preparation of Ni/Nb_2O_5 modified with L-lysine was mainly as follows: 0.1 g of Ni/Nb_2O_5 and different qualities of L-lysine (0.0025, 0.005, 0.01, and 0.02 g, respectively) were ground uniformly in an agate mortar, and the uniformly mixture was maintained for 3 h at 200 °C in a tube furnace with H_2 atmosphere to obtain the target catalyst. The mass ratios of L-lysine and Ni/Nb_2O_5 were 0.025, 0.05, 0.1 and 0.02, respectively.

2.5. Adsorption of n-hexanoic acid or n-hexylamine on the surface of Ni/Nb_2O_5

0.01 g of Ni/Nb_2O_5 and 0.034 mmol of *n*-hexanoic acid or *n*-hexylamine were added in 1 mL of isopropyl alcohol. The obtained mixture was ultrasonically dispersed and dried in a vacuum oven at 80 °C for 12 h. The samples were then characterized by FT-IR and XPS.

2.6. Characterizations

The XRD patterns were tested on a MiniFlex II diffractometer with the conditions of Cu-Kα radiation (λ = 1.5418 Å) and manipulated in a 2θ range of 5–80° at a scanning rate of 8° min^{-1}. The scanning electron microscopy (SEM) images with different multiples were acquired through a JSM-7001 F instrument. For the more detailed surface messages, the transmission electron microscopy (TEM) carried out on a JEM-2100 F microscope with accelerating voltage of 200 kV was used to characterize the obtained samples. To investigate components and the valence state of elements of catalysts, X-ray photoelectron spectroscopy (XPS) was conducted on a Thermo ESCALAB 250 spectrometer at room temperature using an Al Kα X-ray source ($h\nu$ = 1486.6 eV). The C 1*s* peak at 284.6 eV was used as a reference for the calibration of the binding energy scale. To investigate the light adsorption behavior of the samples, the UV-Vis diffuse reflectance (UV-Vis-DR) spectra were measured using a Hitachi U-3900 spectrometer. *In situ* diffuse reflectance infrared Fourier transform spectroscopy (DRIFTs) was used to observe the substrates and intermediates adsorption on the surface of catalysts by Bruker Tensor II spectrometer equipped with a MCT detector. Fourier transform infrared spectra (FT-IR) of samples were also obtained by the Bruker Tensor II spectrometer. The total Ni loadings of various based-Ni catalysts were determined by an inductively coupled plasma (ICP) spectrometer on a Thermo iCAP6300 instrument. The amounts of N elements were measured by elemental analyser (Vario EL CUBE). Thermogravimetric/differential thermal (TG/DTA) analysis was carried out on a Rigaku TG in N_2 with a heating rate of 10 °C min^{-1}. ^1H and ^{13}C NMR spectroscopy was recorded by Bruker AVANCE IIITM spectrometer (frequencies of 400 and 100 MHz) and the chemical shift was referenced to TMS (tetramethylsilane) by using D_2O as the solvent.

2.7. Photocatalytic phenylacetylene hydrogenation to styrene

Typically, 10 mg of catalyst and 2 mL of phenylacetylene in isopropyl alcohol solution (0.05 M) were added into a 10 mL vial. The vial was then purged with H_2 for 1 min to maintain the H_2 pressure at 1 atm and kept at 80 °C in an oil bath for 6 h under visible light irradiation (white LED, 600 mW cm^{-2}). After that, the catalyst was filtered with a 0.22 mm nylon syringe filter and the products were analyzed using a Shimadzu 2014 C gas chromatography equipped with a WondaCap 5 column. The amount of products and reactants was calculated using an external standard method. The calculation formula for conversion and selectivity is as follows [*n*(mol), amount of substance].

$$\text{Conversion} = [n_{(\text{product 1})} + n_{(\text{product 2})\cdot}]/n_{(\text{reactant})} \times 100\%$$

$$\text{Selectivity} = [n_{(\text{product})}/(n_{(\text{product 1})} + n_{(\text{product 2})\cdot})] \times 100\%\cdot$$

2.8. Computation details

Based on the density functional theory (DFT), all of the computations are performed by employing the generalized gradient approximation (GGA) [33] with the Perdew-Burke-Ernzerhof exchange-correlation functional within the frame of Vienna *ab initio* simulation package (VASP) [34,35]. A 400 eV cutoff is employed for the plane-wave basis set. A semi-empirical van der Waals (vdW) correction is used to account for the dispersion interactions [36], and the projector-augmented plane wave (PAW) is used to describe the electron-ion interactions [37,38]. The geometrical optimization of bulk Ni structure is carried out using 7 × 7 × 7 Monkhorst-Pack grid *k*-points. Based on the optimized 3D structure, we simulated the Ni(111) surface by the slab with three atomic layers. For all the studied slab systems, 3 × 3 × 1 *k*-points are adopted for the structural optimizations, where the two atomic layers below are frozen and the remaining atoms are relaxed during the calculation process. For all computations, the convergence threshold is set as 10^{-4} eV in energy.

Moreover, the adsorption energy involved in this work can be computed by the following equation : .

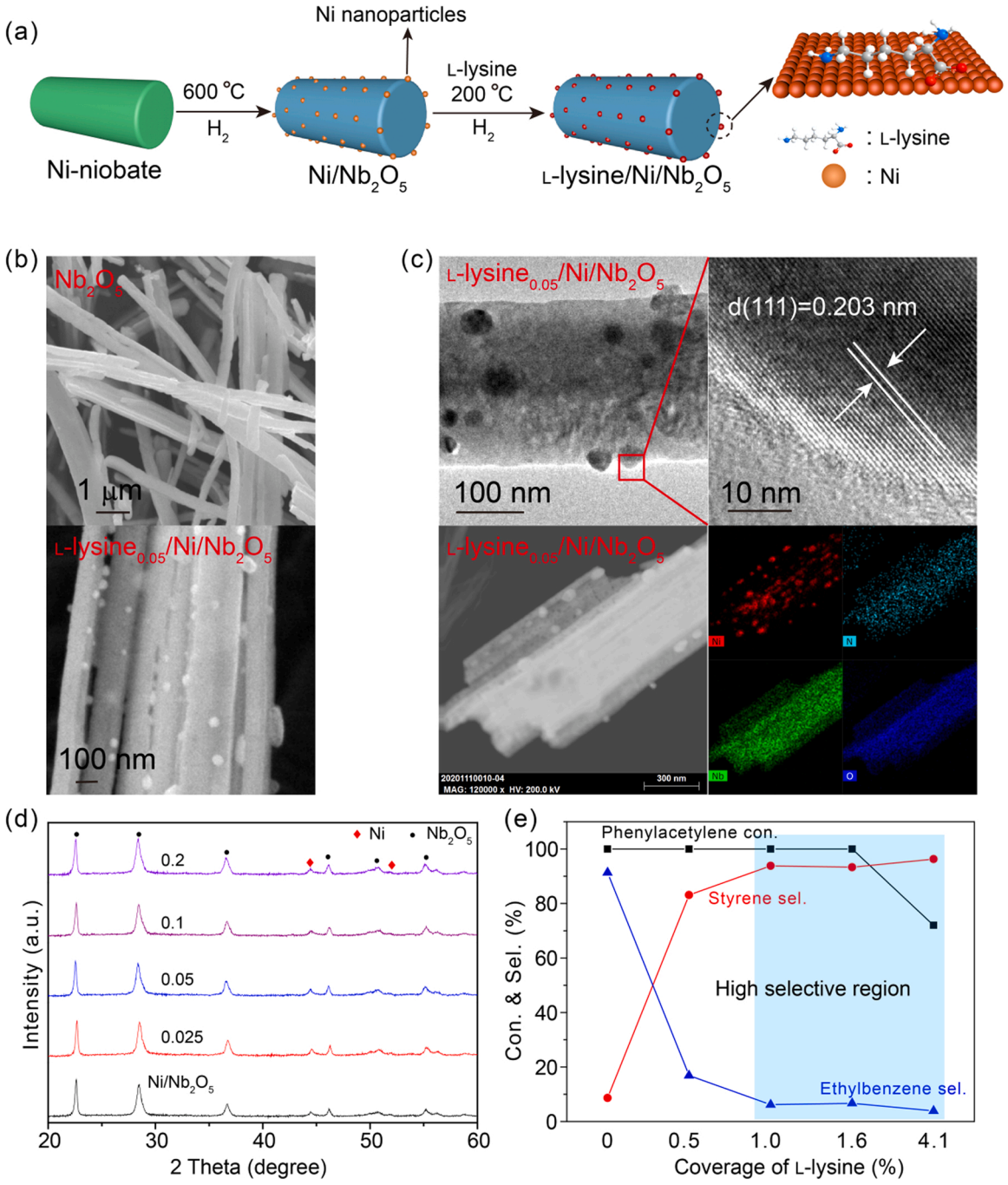

Fig. 1. Synthesis, characterization and photocatalytic performance of L-lysine modified Ni/Nb_2O_5. (a) Schematic diagram showing the preparation of L-lysine modified Ni/Nb_2O_5. (b) SEM images of Nb_2O_5 and L-$lysine_{0.05}/Ni/Nb_2O_5$. (c) TEM, HRTEM, STEM and elementary mapping images of L-$lysine_{0.05}/Ni/Nb_2O_5$. (d) XRD patterns of L-lysine/Ni/Nb_2O_5 with different mass ratio of L-lysine to Ni/Nb_2O_5. (e) Influence of coverage of L-lysine to Ni/Nb_2O_5 on phenylacetylene hydrogenation. Reaction conditions: photocatalyst, 10 mg; temperature, 80 °C; time, 12 h; isopropyl alcohol, 2 mL; phenylacetylene, 0.1 mmol; H_2, 1 atm; white LED, 600 mW cm^{-2}.

$\Delta E_{ads} = E_{slab} + E_X - E_{total}$

where E_{total} and E_{slab} are the total energies of the studied system with and without the adsorbate, and E_X is the energy of adsorbed molecule.

3. Results and discussion

3.1. Structure analysis and selective hydrogenation performance of L-lysine modified Ni/Nb_2O_5

The typical preparation process of L-lysine$_x$/Ni/Nb_2O_5 (x is the corresponding mass ratio of L-lysine and Ni/Nb_2O_5) catalyst is shown in Fig. 1a. Nb_2O_5 exhibits a fibril morphology as observed from the SEM image (Fig. 1b). The SEM and TEM images of classical L-lysine$_{0.05}$/Ni/Nb_2O_5 show that Ni NPs with an average particle size of 31.5 nm are uniformly distributed on the surface of the Nb_2O_5 fiber (Fig. S1). The HRTEM image shown in Fig. 1c proves the existence of Ni(111) plane with a d-spacing of 0.203 nm. The EDX elementary mapping shows that the N element of L-lysine is uniformly distributed on the surface of Ni/Nb_2O_5 besides Ni, Nb and O elements of L-lysine$_{0.05}$/Ni/Nb_2O_5. The existing form of L-lysine on the catalyst is characterized by Fourier transform infrared spectra (FT-IR) analysis (shown in the next section). The XRD diffraction peaks of Ni/Nb_2O_5 modified with different amounts of L-lysine molecules all show the mixture of metallic Ni (JCPDS no. 87–0712) and Nb_2O_5 (JCPDS no. 71–0336). And the diffraction peaks of metallic Ni exhibit no obvious change with the increase of the starting material L-lysine compared with that of the original Ni/Nb_2O_5 (Fig. 1d), suggesting that L-lysine modification strategy cannot affect the crystal structure of Ni NPs on the surface of Nb_2O_5.

The photocatalytic performance of various catalysts in phenylacetylene hydrogenation reaction are studied. It is obvious that L-lysine modification strategy can remarkably increase styrene selectivity with the increase of the coverage of L-lysine to Ni/Nb_2O_5 (Fig. 1e). In which, the coverage of L-lysine on the surface of Ni nanoparticles (NPs) is taken as the molar ratio of L-lysine to Ni nanoparticles measured by inductive coupled plasma emission spectrometer (ICP) and element analyzer (EA) (Table S1). It is obvious that L-lysine modification strategy can remarkably increase styrene selectivity with the increase of coverage of L-lysine on the surface of Ni NPs from 0% to 1.0%. When the coverage of L-lysine on the surface of Ni NPs is 4.1%, the selectivity of styrene does not decrease, but the conversion of phenylacetylene decreased. This may be caused by the decrease of phenylacetylene adsorption sites due to the increase of the coverage of L-lysine on the surface of Ni NPs. Hence, the results indicate the importance of the coverage of L-lysine on Ni nanoparticles in regulating styrene selectivity over Ni/Nb_2O_5.

In the control experiment, Ni/Nb_2O_5 without L-lysine modification shows low styrene selectivity (7.2%, Table 1, entry 1) with > 99.9% of phenylacetylene conversion. The styrene selectivity can be increased to 95.8% at full conversion of phenylacetylene when the mass ratio of L-lysine to Ni/Nb_2O_5 is 0.05 (the coverage of L-lysine is 1.0%, Table S1, entry 2). This ratio is fixed if no specific definition. To demonstrate the function of carboxyl and amino groups of L-lysine, 200 °C modification method and isopropyl alcohol solution modification are selected. And the detailed discussion is shown in supporting. For example, the hydrogenation of phenylacetylene is carried out over Ni/Nb_2O_5 catalyst modified with *n*-hexylamine, *n*-hexanoic acid and 1-aminohexanoic acid using isopropyl alcohol solution modification method, respectively (Table 1, entries 3–5). It can be clearly found that both *n*-hexylamine and 1-aminohexanoic acid can regulate hydrogenation of phenylacetylene to styrene. However, *n*-hexanoic acid hardly modulate the selectivity of styrene and affect the conversion of phenylacetylene. Meanwhile, L-lysine modulated Ni/Nb_2O_5 [Ni/Nb_2O_5(L-lysine)] is prepared using same preparation method with Ni/Nb_2O_5(*n*-hexanoic acid) and Ni/Nb_2O_5(*n*-hexylamine) to eliminate the influence of preparation method. It can be found that 97.3% of high styrene selectivity at 12 h for Ni/Nb_2O_5(L-lysine) is shown (Table 1, entry 6). And the styrene selectivity at 96.7% can still maintain by prolonging the time to 72 h (Table 1, entry 7). These results indicate that there is no work to modulate the selectivity of styrene for carboxyl groups of L-lysine, while amino group of L-lysine mainly interact with metallic Ni to modulate selectivity of styrene.

3.2. Bidentate ligand in L-lysine co-anchoring on Ni towards simultaneously enhanced stability

In the control experiment, the photocatalytic stability of Ni/Nb_2O_5 adsorbing *n*-hexylamine molecules [Ni/Nb_2O_5(*n*-hexylamine)] and L-lysine$_{0.05}$/Ni/Nb_2O_5 are evaluated (Fig. 2a–c). It is shown that Ni/Nb_2O_5(*n*-hexylamine) exhibits poor stability (Fig. 2a). But high stability is observed for L-lysine$_{0.05}$/Ni/Nb_2O_5 (Fig. 2b). The XRD pattern of recycled L-lysine$_{0.05}$/Ni/Nb_2O_5 has no obvious change compared to that of fresh L-lysine$_{0.05}$/Ni/Nb_2O_5 (Fig. S2a). Meanwhile, the FT-IR

Table 1
Photocatalytic performance of various catalysts for phenylacetylene hydrogenation.

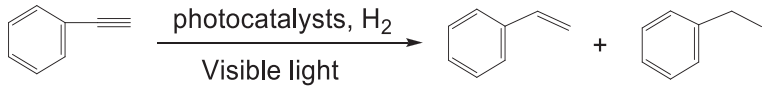

a b c

Entry	Catalysts	Con. (%)	Sel. (%)	
			b	c
1	Ni/Nb_2O_5	> 99.9	7.2	92.8
2	L-lysine/Ni/Nb_2O_5	> 99.9	95.8	4.2
3	Ni/Nb_2O_5(*n*-hexylamine)	> 99.9	95.3	4.7
4	Ni/Nb_2O_5(*n*-hexanoic acid)	> 99.9	14.5	85.5
5	Ni/Nb_2O_5(1-aminohexanoic acid)	> 99.9	94.3	5.7
6	Ni/Nb_2O_5(L-lysine)	58.5	97.3	2.7
[d]7	Ni/Nb_2O_5(L-lysine)	> 99.9	96.7	3.3
8	L-lysine/Ni/Nb_2O_5 (150 °C)	7.8	96.9	3.1
9	L-lysine/Ni/Nb_2O_5 (25 °C)	7.4	97.3	2.7
10	NiO/Ni/Nb_2O_5	12.1	95.7	4.3
11	NiO/Nb_2O_5	2.0	99.9	n.d.
12	Ni powder	12.2	95.5	4.5
13	Ni foam	4.2	99.9	n.d.
14	Nb_2O_5	n.d.	n.d.	n.d.

Reaction conditions: photocatalysts, 10 mg; temperature, 80 °C; time, 12 h; isopropyl alcohol, 2 mL; phenylacetylene, 0.1 mmol; H_2, 1 atm; white LED, 600 mW cm^{-2}. n.d. = not detected. [d]Reaction time is 72 h.

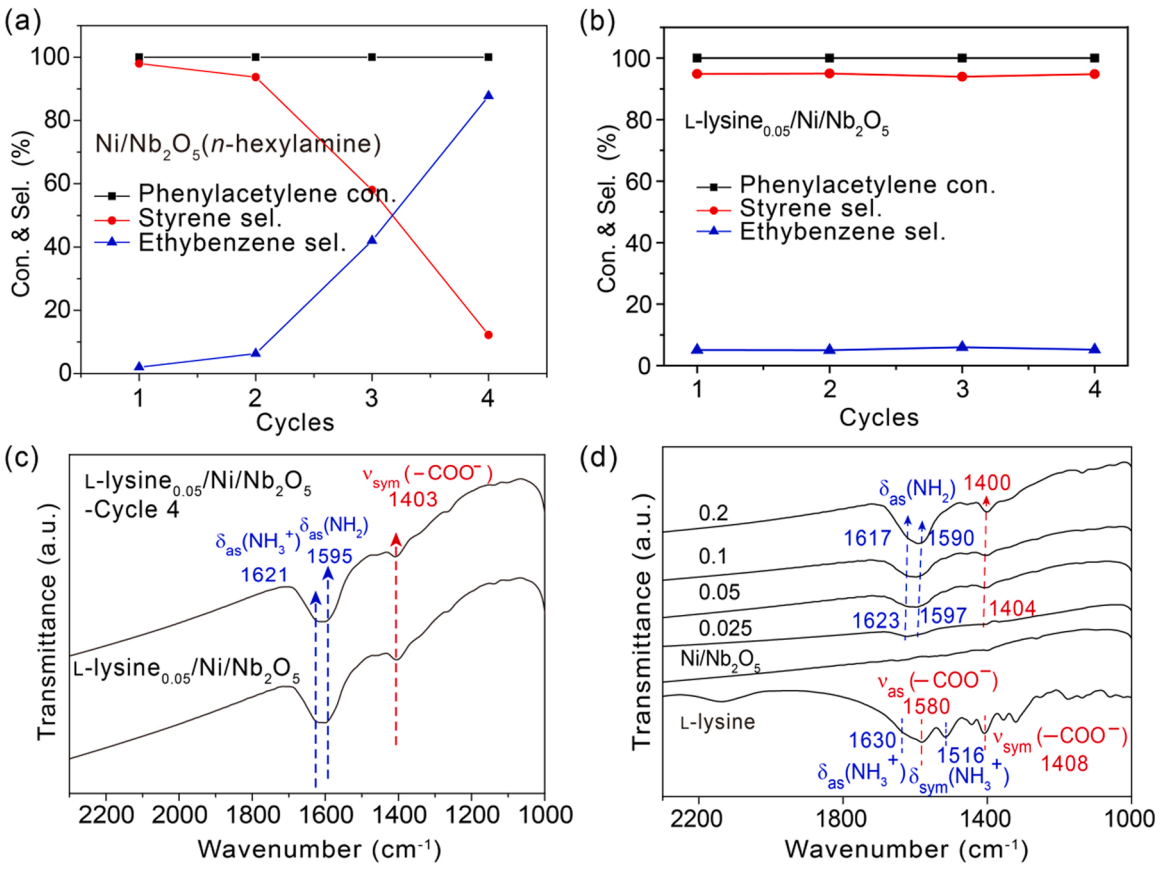

Fig. 2. Recognition of L-lysine molecules adsorption and stability on the surface of Ni/Nb_2O_5. The photocatalytic stability of (a) Ni/Nb_2O_5(*n*-hexylamine) and (b) L-$lysine_{0.05}/Ni/Nb_2O_5$ in four cycles. Reaction conditions: phenylacetylene, 0.1 mmol; photocatalyst, 10 mg; isopropyl alcohol 2 mL; H_2, 1 atm; temperature, 80 °C; white LED, 600 mW cm^{-2}; 6 h. (c) FT-IR spectra of L-$lysine_{0.05}/Ni/Nb_2O_5$ before and after reaction. (d) FT-IR spectra of Ni/Nb_2O_5 and L-lysine/Ni/Nb_2O_5 with different mass ratio of L-lysine and Ni/Nb_2O_5.

characteristic peaks of L-lysine are well preserved for the recycled L-$lysine_{0.05}/Ni/Nb_2O_5$ (Fig. 2c, the recognition of L-lysine molecules will be discussed in the following paragraph). In addition, the thermal analysis is conducted to study the thermal stability of L-lysine modified catalyst. The TG and DTA curves of L-lysine show the classic endothermic peak at 226.5 °C attributed to the melting point of L-lysine [39], confirming that L-lysine molecules are very stable and no polymerization or decomposition occurs at 200 °C (Fig. S3a). Meanwhile, the weak endothermic peak at 260.3 °C attributed to the decomposition of L-lysine of L-$lysine_{0.05}/Ni/Nb_2O_5$ is also shown in Fig. S3b, demonstrating the stability of L-$lysine_{0.05}/Ni/Nb_2O_5$. ^1H NMR spectra of L-lysine molecules before and after heat treatment at 200 °C are shown in Fig. S3c. The typical proton signals for –CH and $–CH_2$ are all observed except for that of $–NH_3^+$ and $–NH_2$ group because of the fast deuterium exchange in D_2O solvent [39]. The changes for $–CH_2$ for the L-lysine heat-treated at 200 °C can be caused by hydrogen bonds between the terminal amino groups of L-lysine molecules [40]. Hence, the L-lysine molecules can be stably present on the surface of Ni/Nb_2O_5 at 200 °C.

The recognition of L-lysine molecules on the surface of Ni/Nb_2O_5 and the strong interaction between L-lysine molecules and Ni/Nb_2O_5 are proved by FT-IR in Fig. 2d. The $–NH_3^+$ asymmetric bending vibration peak at 1630 cm^{-1}, the $–COO^-$ asymmetric stretching vibration peak at 1580 cm^{-1} and the $–COO^-$ symmetric stretching vibration peak at 1408 cm^{-1} are shown [40], impling that the pristine L-lysine molecules are mainly in the zwitterionic form. It can be clearly found that the asymmetric stretching peak of $–NH_3^+$ shifts from 1630 to 1623 cm^{-1} and a new asymmetric stretching peak of $–NH_2$ appears at 1597 cm^{-1}, when the mass ratio of L-lysine and Ni/Nb_2O_5 is 0.025 [40,41]. At the same time, the symmetric stretching vibration peak of $–COO^-$ shifts from 1408 to 1404 cm^{-1} and there is no appearance for asymmetric stretching vibration peak of $–COO^-$. This can be ascribed to reorientation of the terminal amine group of L-lyisne because of the influence of temperature, and the zwitterionic form of L-lysine is also retained due to high coverage of L-lysine [40]. When further increasing mass ratio to 0.2, the characteristic peaks of $–NH_3^+$, $–NH_2$ and $–COO^-$ shifts from 1623 to 1617 cm^{-1}, 1597–1590 cm^{-1} and 1404–1400 cm^{-1}, respectively. Meanwhile, when the mass tatio is 0.2, the relative strength of asymmetric bending peak of $–NH_3^+$ almost disappears while the asymmetrical stretching vibration peak of $–NH_2$ and asymmetrical stretching vibration peak of $–COO^-$ are mainly displayed. These results illustrate that the interaction between $–NH_2$ and $–COO^-$ groups of L-lysine and Ni/Nb_2O_5 is dominant with the increase of mass ratio of L-lysine and Ni/Nb_2O_5, while the interaction between $–NH_3^+$ and $–COO^-$ of L-lyisne and Ni/Nb_2O_5 is also present.

The strong interaction between Ni/Nb_2O_5 and L-lysine molecules is further confirmed by XPS analysis, in which the binding energies of Ni 2*p*, Nb 3*d*, O 1*s*, N 1*s* and C 1*s* are obtained (Fig. S4aFig. S4a–e). Compared with the binding energy at 852.6 eV of metallic Ni of the original Ni/Nb_2O_5 [15,42–45], the binding energies of metallic Ni $2p_{3/2}$ of Ni/Nb_2O_5 modified with different amounts of L-lysine gradually shift from 852.3 to 851.6 eV (Fig. S4a), implying that L-lysine molecules have strong interaction with Ni/Nb_2O_5, leading to more enriched electrons around metallic Ni. At the same time, the corresponding binding energies of Nb $3d_{3/2}$ and $3d_{5/2}$ migrated from 210.1 to 209.4 eV and 207.3–206.6 eV (Fig. S4b) [32], respectively, confirming that L-lysine molecules also can interact with Nb_2O_5 (also demostrated in Fig. S5) and make electrons around Nb more enriched. Correspondingly, the binding energy of O 1*s* of –C═O decreases from 531.6 to 531.1 eV (Fig. S4c), the

binding energy of N 1*s* of –NH gradually decreases from 399.8 eV to 399.4 eV (Fig. S4d), the binding energy of C 1*s* of –C═O decreases from 288.6 to 287.8 eV, and the binding energy of C 1 *s* of C–N increases from 285.4 to 285.8 eV (Fig. S4e). Meanwhile, the hybridization of N- or O-2*p* and Ni-3*d* orbitals is analyzed for the most sable configuration L-1 (demonstrated in Fig. 3), the adsorbed L-lysine can lie down the Ni(111) surface, where the N atom in $–NH_2$ group and O atom in $–COO^-$ group are bonded to the Ni atoms on the surface to form the Ni–N and Ni–O chemical bonds by the way that the electrons around Ni are attracted by the N and O of L-lysine (Fig. 3b). The calculated Ni–N and Ni–O bond lengths can be 2.043 and 2.001 Å, respectively. The formation of Ni–N and Ni–O bonds can be also supported by the computed results of partial density of states (PDOS), in which the N- or O-2*p* and Ni-3*d* orbitals have obvious hybridization (Fig. 3c). In addition, the electron density of metallic Ni can be affected by the outer electron orbits [32,46], leading to co-increasing of binding energies of O 1*s* and N 1*s* of L-lysine and Ni $2p_{3/2}$ of metallic Ni. And the increase of the binding energies of the corresponding C connected to the $–COO^-$ and –NH groups is mainly because the $–COO^-$ and –NH of L-lysine can attract surrounding electrons of C. This result combined with that of FT-IR confirms that there is a strong interaction between Ni NPs and the $–COO^-$ and $–NH_2$ groups of the L-lysine molecules.

To figure out the adsorption mode of L-lysine on the metallic Ni as the active center, various adsorption modes of L-lysine molecule on the surface of metallic Ni are optimized and corresponding adsorption energies are calculated by considering possible spatial conformations (Fig. 3a). The computed results reveal that a total of three configurations can be achieved (Fig. 3a), among which the configuration L-1 can exhibit the largest adsorption energy ($\Delta E_{ads} = 2.892$ eV), indicating the highest structural stability. Moreover, for the purpose of comparison, the adsorption of the *n*-hexylamine with the similar structure but the chain end modified by only NH_2 group is also considered (Fig. 3a). The results show that two adsorption configurations of *n*-hexylamine can be obtained on the Ni(111) surface, where the configuration H-1 (1.742 eV) has larger adsorption energy than the configuration H-2 (1.453 eV), in view of the formation of Ni-N bond. However, the adsorption energy of H-1 (1.742 eV) can be much smaller than that of L-1 (2.892 eV), indicating that L-lysine can be anchored on the Ni(111) surface more effectively, due to the simultaneous existence of both the Ni–N and Ni–O bonds. This result combined with the fact that *n*-hexanoic acid does not affect the activity of the active metal Ni (Table 1, entry 4), suggesting that the strong co-interaction between $–NH_2$ and $–COO^-$ groups of L-lysine and Ni/Nb_2O_5 is favorable to improve stability of L-lysine/Ni/Nb_2O_5, while amino group of L-lysine mainly interact with metallic Ni to modulate selectivity of styrene [47].

To further illustrate the interaction for physical mixing of L-lysine

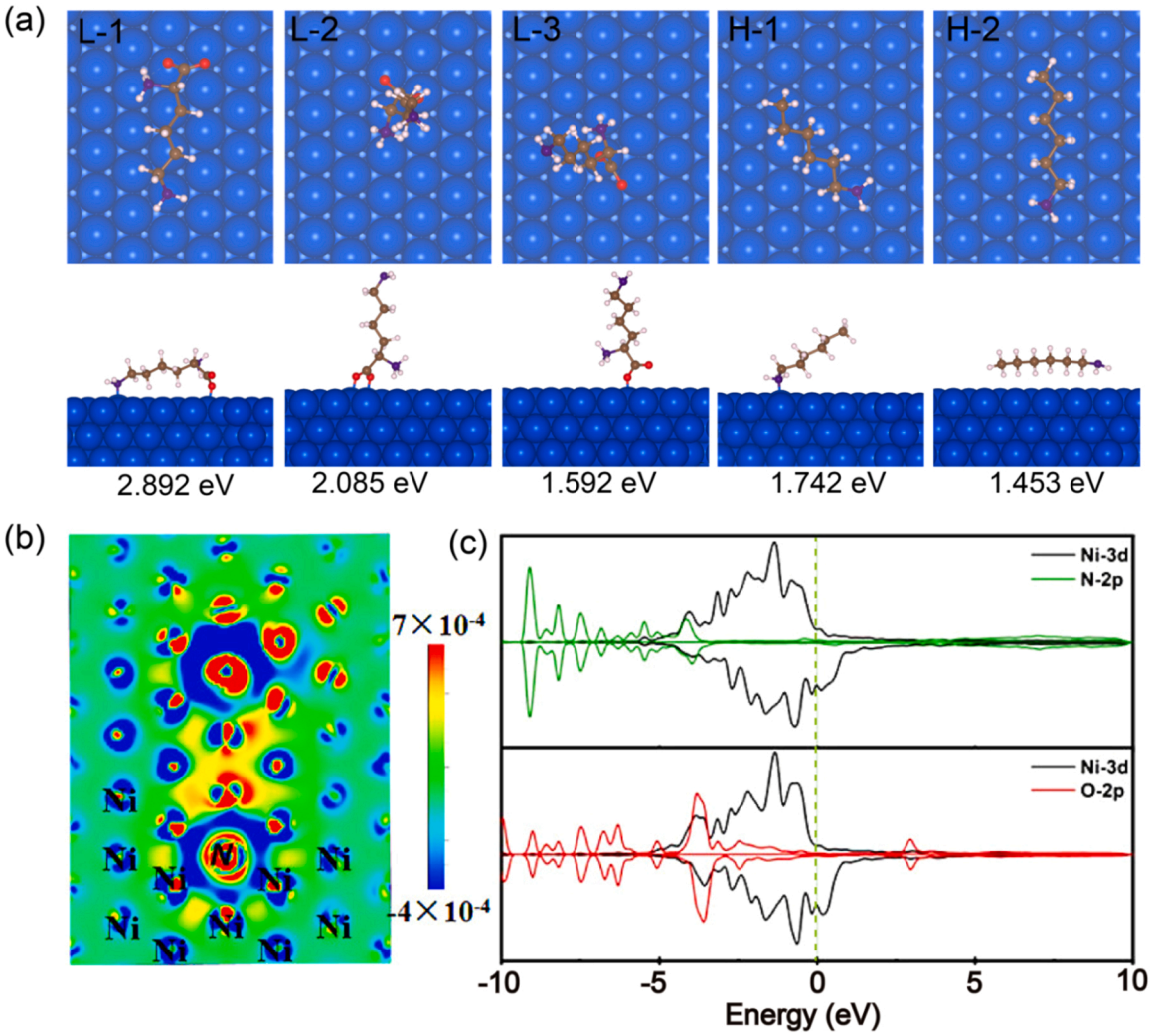

Fig. 3. Adsorption mode of L-lysine (bidentate ligand) and *n*-hexylamine (monodentate ligand) on the surface of metallic Ni. (a) Top and side views of the optimized structures with L-lysine (L-1 ~ L-3) and *n*-hexylamine (H-1 and H-2) on the different adsorption positions of Ni(111) surface. Red ball, O; grey ball, H; brown ball, C; blue ball, N. (b) The charge density difference ($\Delta\rho$) for L-1 structure, where the blue and red areas mean that the electron density decreases and increases, respectively. (c) Partial density of states (PDOS) for L-1 structure.

and Ni/Nb_2O_5, it is shown for XPS and FT-IR spectra of Ni/Nb_2O_5 regulated by L-lysine molecules at different temperatures in Fig. S6. It can be found that the binding energy of metallic Ni does not change significantly during physical mixing (Fig. S6a). With the increase of temperature, the binding energy of metallic Ni gradually decreases from 284.6 to 284.2 eV, indicating there is no strong interaction between L-lysine and metal Ni NPs for simple physical mixing of L-lysine and Ni/Nb_2O_5. Meanwhile, FT-IR spectra of L-lysine$_{0.05}/Ni/Nb_2O_5$ prepared at different temperatures are shown in Fig. S6b to illustrate the interaction between L-lysine and Ni/Nb_2O_5. It can be found that the characteristic peaks of the pristine L-lysine are only displayed at the stage of physical mixture of Ni/Nb_2O_5 and L-lysine. The characteristic peaks of the $–NH_3^+$ and $–COO^-$ groups shift significantly when the preparation temperature reaches a higher temperature. New characteristic peak of the $–NH_2$ group at 1596 cm^{-1} appears at 150 °C. When preparation temperature rises to 200 °C, new characteristic peak of the $–NH_2$ group shifts to lower wavenumber at 1595 cm^{-1}, the characteristic peak of $–NH_3^+$ group decreases to 1621 cm^{-1} and the characteristic peak of $–COO^-$ group shifts to 1403 cm^{-1}. These results indicate that the strong interaction between both $–NH_2$ and $–COO^-$ groups of L-lysine molecules and Ni/Nb_2O_5 can be achieved under high temperature conditions, and the interaction between L-lysine molecule and metal Ni particles after physical mixing mainly depends on $–NH_3^+$ and $–COO^-$ group of L-lysine molecule. Moreover, L-lysine$_{0.05}/Ni/Nb_2O_5$ with preparation temperature below 200 °C (e.g. 150 and 25 °C) shows very low conversion of phenylacetylene (Table 1, entries 8 and 9), indicating that high selectivity of styrene at full conversion of phenylacetylene can be achieved when both $–NH_2$ and $–COO^-$ groups of L-lysine interact with Ni/Nb_2O_5.

3.3. Light enhanced H_2 activation over metallic Ni NPs

The relationship between photocatalytic activity and incident light intensity is investigated using L-lysine$_{0.05}/Ni/Nb_2O_5$ to clarify the function of visible light. As shown in Fig. S7a, when light intensity increases from 300 to 600 mW cm^{-2}, the light irradiation contribution increases from 44.9% to 76.9%. The kinetics of different temperatures (70, 80 and 90 °C) are also carried out to calculate the activation energies in the presence or absence of light, which is favorable to clarify the increase of photocatalytic performance using L-lysine$_{0.05}/Ni/Nb_2O_5$ catalyst (Fig. S8). The reaction rate constants at different temperatures under light or dark conditions are obtained (Fig. S8a and b). The calculated activation energy of phenylacetylene over L-lysine$_{0.05}/Ni/Nb_2O_5$ under light irradiation is 88.1 kJ mol^{-1} (Fig. S8c), which is remarkably lower than that (112.3 kJ mol^{-1}, Fig. S8d) in the dark according to the Arrhenius equation [48]. The significant decrease in the activation energy further confirms that light can facilitate conversion of phenylacetylene.

According to the previous report [49–52], photoexcited metal electrons accelerated reactions mainly through photothermal effect and electron transfer mechanism. Hence, the action spectrum (the performance under different wavelength of light) is conducted over L-lysine$_{0.05}/Ni/Nb_2O_5$ (Fig. S7b). The strong LSPR effect of metallic Ni NPs is also observed in all L-lysine modified Ni/Nb_2O_5 (Fig. S7c) [29,53]. Apparently, the apparent quantum yield (AQY) values track with the UV-Vis diffuse reflectance spectrum of L-lysine$_{0.05}/Ni/Nb_2O_5$, in which a broad peak centered at about 550 nm is attributed to the typical plasmonic absorption of metallic Ni NPs. This result is consistent with the wavelength-dependent performances over Ni/Al_2O_3 for CO_2 reduction, which is driven from the LSPR effect of Ni NPs [29]. The result suggests that phenylacetylene hydrogenation reaction is predominately driven by photoexcited electrons transfer in virtue of LSPR effect of metallic Ni NPs.

To further demonstrate the viewpoint and exclude the photothermal effects, actual reaction temperatures with or without L-lysine$_{0.05}/Ni/Nb_2O_5$ under visible light irradiation are measured and the corresponding photocatalytic activities are evaluated (Fig. S9). When the set temperatures of oil bath are 40 , 60 and 80 °C, the temperature of reaction solution increase to 65 , 75 , and 83 °C with L-lysine$_{0.05}/Ni/Nb_2O_5$ under visible light irradiation (Fig. S9a–c). Typically, when actual temperature of reaction solution is 80 °C without visible light irradiation, the phenylacetylene conversion is around 20%, far lower than the conversion at 80 °C under visible light irradiation (Fig. S9d). These results demonstrate that light can indeed increase the temperature of the reaction solution, but it cannot achieve the high activity under light irradiation. Hence, the increased photoactivity of phenylacetylene hydrogenation over L-lysine$_{0.05}/Ni/Nb_2O_5$ is mainly attributed to photoexcited electron transfer of metal Ni.

To demonstrate the key role of the Ni^{2+} or metallic Ni NPs, NiO/Nb_2O_5 and $NiO/Ni/Nb_2O_5$ catalysts comprising metallic and/or oxidized Ni are also prepared with Ni-niobate as precursor [32] and demonstrated by XRD, TEM, HRTEM and XPS in Fig. S10–14. $NiO/-Ni/Nb_2O_5$ and NiO/Nb_2O_5 are prepared by calcination of Ni/Nb_2O_5 in Air for 2 h at 200 °C and 500 °C, respectively. As detected by inductively coupled plasma mass spectrometry (ICP), the Ni contents of Ni/Nb_2O_5, NiO/Nb_2O_5, and $NiO/Ni/Nb_2O_5$ catalysts are 6.3 wt%, 6.6 wt%, and 6.3 wt% (Table S2, entries 1–3), respectively. And the statistical particle size of Ni NPs for Ni/Nb_2O_5 is about 30.4 nm (Fig. S10b). Ni/Nb_2O_5 shows the highest phenylacetylene conversion (>99.9%) with poor styrene selectivity (7.2%) under visible light irradiation at 12 h compared with NiO/Nb_2O_5 and $NiO/Ni/Nb_2O_5$ (Table 1, entries 1 and 10–11), indicating that metallic Ni plays a vital role in the enhancement of photocatalytic performance, but it does not work for Ni^{2+} in the reaction system of photocatalytic hydrogenation of phenylacetylene to styrene. The reaction cannot proceed without Ni/Nb_2O_5 both in dark and light, indicating that Ni/Nb_2O_5 photocatalyst is necessary for the selective hydrogenation of phenylacetylene. In addition, as the Ni loading of Nb_2O_5 increases, phenylacetylene conversion gradually increases (Fig. S11a–b). The good photocatalytic performances of Ni-based catalysts with different supports are also shown in Table S4. Commercial Ni power or Ni foam shows poor photocatalytic performance (Table 1, entries 12 and 13), illustrating that it is important that Ni NPs are dispersed on the surface of supports. These results further demonstrate that metallic Ni is the active center to increase photocatalytic performance for selective hydrogenation of phenylacetylene.

There are no phenylacetylene or styrene conversion when reaction is conducted in Ar over Ni/Nb_2O_5 catalyst, indicating the active hydrogen species are ascribed to H_2 rather than isopropyl alcohol. In addition, no reaction occurs over Nb_2O_5 in H_2 atmosphere (Table 1, entry 14). The results suggest that metallic Ni plays a crucial role in activating H_2.

The H_2 activation process is schematically shown and clarified with or without light irradiation using *in situ* DRIFTs in Fig. 4a. With time increased from 0 to 140 min, the obvious bands at 2973, 2934 and 2861 cm^{-1} can be assigned to the stretching vibration of $–CH_x$ ascribed to the product of residual CO_2 methanation with H_2 in 80 °C in the dark, indicating that H_2 can be dissociated homolytically on the surface of Ni NPs [9]. However, when H_2 activation experiment is conducted under light irradiation, the intensity of stretching vibration peaks of $–CH_x$ at 30 min is obviously higher than that at 140 min in dark, indicating light can facilitate H_2 activation on the surface of Ni and the production of $–CH_x$ because of the fast methanation process. The results indicate that light can excite electrons of metal Ni by LSPR effect of Ni NPs to induce H_2 activation quickly and then increase the phenylacetylene conversion.

3.4. Proposed selective control and reaction mechanism

Firstly, the kinetics of the phenylacetylene hydrogenation reaction over Ni/Nb_2O_5 and L-lysine$_{0.05}/Ni/Nb_2O_5$ are studied (Fig. S15). It can be clearly found that the selectivity of styrene is still maintained about 94.1% after the conversion of phenylacetylene reaches 95.7% at 6 h over Ni/Nb_2O_5 under visible light irradiation (Fig. S15a). However, the selectivity of ethylbenzene has reached more than 90% at 12 h. Amazingly, the styrene selectivity (around 95%) can be maintained all the

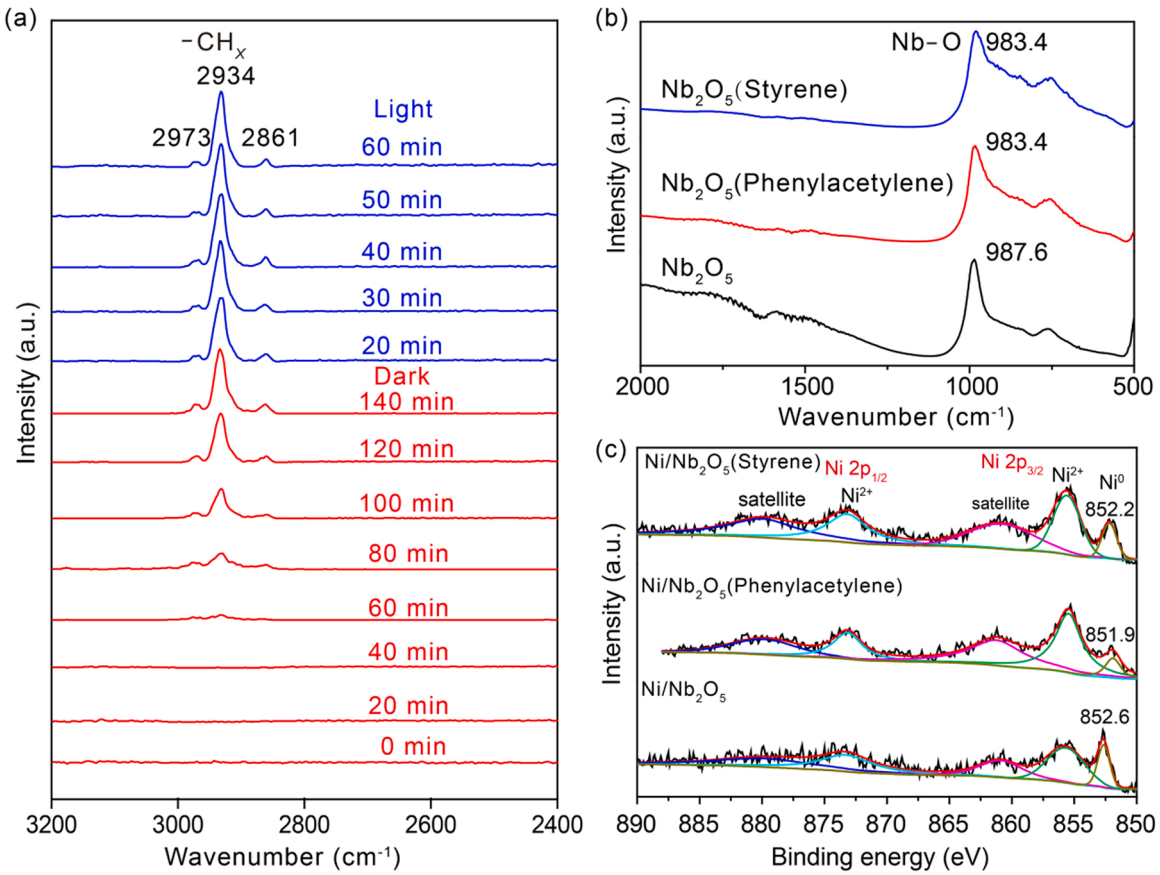

Fig. 4. Observation of H_2 activation process and the interaction between phenylacetylene/styrene and catalyst surface. (a) H_2 activation on the surface of L-lysine$_{0.05}$/Ni/Nb_2O_5 in dark and light. (b) DRIFTs of phenylacetylene and styrene adsorbed on Nb_2O_5, respectively. (c) Ni 2*p* XPS spectra of Ni/Nb_2O_5 after phenylacetylene and styrene adsorption, respectively.

time with L-lysine$_{0.05}$/Ni/Nb_2O_5 under visible light irradiation (Fig. S15b). The result suggests that Ni/Nb_2O_5 catalyst can only control the selectivity of styrene by controlling the time, and L-lysine is very important to maintain the selectivity of styrene.

Hence, in order to further study whether metallic Ni or Nb of Ni/Nb_2O_5 is preferential active site of phenylacetylene or styrene hydrogenation, the DRIFTs of two molecules adsorbed on the surface of Nb_2O_5 are shown in Fig. 4b. Identical variation of the infrared stretching vibration peak of Nb−O of Nb_2O_5 can be observed when adsorbing the phenylacetylene or styrene, indicating that preferential adsorption and activation of substrate molecules on the surface of Nb_2O_5 is impossible. To investigate the influence of phenylacetylene and styrene on metallic Ni, XPS spectra of Ni/Nb_2O_5(phenylacetylene) and Ni/Nb_2O_5(styrene) are shown in Fig. 4c. It can be found that when Ni/Nb_2O_5 absorbs phenylacetylene or styrene, the binding energy of metallic Ni shifts from 852.6 to 851.9 or 852.2 eV, respectively, indicating the strong adsorption between phenylacetylene and metallic Ni, which can be also supported by our DFT calculations. Specifically, the computed results reveal that the styrene can be stably adsorbed on the pure Ni(111) surface with the large adsorption energy as 3.221 eV (I, Fig. S16a), where all the C atoms can be alternately located over the top sites of Ni atoms and over the hollow sites Ni-Ni-Ni, with a distance about 2.000 Å between the molecular and Ni surfaces. Comparatively, when depositing the phenylacetylene on the pure Ni(111) surface (II, Fig. S16b), larger adsorption energy (4.078 eV) can be observed, where all six C atoms in benzene ring can also be alternately located at the top sites of Ni atoms and the hollow sites Ni-Ni-Ni with a distance about 1.989 Å between the molecular and Ni surfaces, while the remaining two C atoms in acetylene part lie at the hollow sites Ni-Ni-Ni with a shorter distance of 1.339 Å, indicating the stronger adsorption interaction. The results suggest that a stronger interaction between phenylacetylene and metallic Ni is clarified, which is in accordance with the result that the adsorption energy (1.81 eV) to 1,2-diphenylethyne reactant of Ni(111) is higher than that (0.99 eV) to *E*-stilbene [24]. Therefore, the metallic Ni active center preferentially activates phenylacetylene molecules in the early stage of photocatalytic reaction, while styrene continues to be activated and hydrogenated in the late stage of the reaction for Ni/Nb_2O_5 catalysts.

Based on the most stable L-1 structure, we further investigate the adsorptions of styrene and phenylacetylene on the Ni(111) surface functionalized by L-lysine to reveal the nature that L-lysine can control the selectivity of styrene (Fig. 5a). When adsorbing styrene and phenylacetylene near the $-NH_2$ group on the surface of L-lysine modified Ni (111), similar structural features can be observed with that on the surface of pure Ni(111), but the correlative distances between the molecules and Ni surface are longer (about 0.040 Å for the former and 0.033 Å for the latter) than the original distances. As a result, their calculated adsorption energies (2.671 and 3.639 eV, respectively) can become smaller than the corresponding those of pristine Ni(111) surface, but the difference between them increases, which improves the selectivity for styrene. This can be mainly due to the evident electron transfer between the Ni(111) surface and the NH_2 group in L-lysine (Fig. 3b), which can effectively modulate the electron density of Ni atoms near the $-NH_2$ group. Moreover, such the large adsorption energies for styrene and phenylacetylene on the L-lysine modified Ni(111) surfaces can be mainly attributed to the effective hybridization between the 2*p* orbitals of correlative C and 3*d* orbitals of Ni atoms, as revealed the computed DOS results (Fig. 5b). Overall, employing L-lysine can effectively functionalize the Ni(111) surface, which can be considered as an effective strategy to improve the selectivity of styrene and ensure the high structural stability simultaneously.

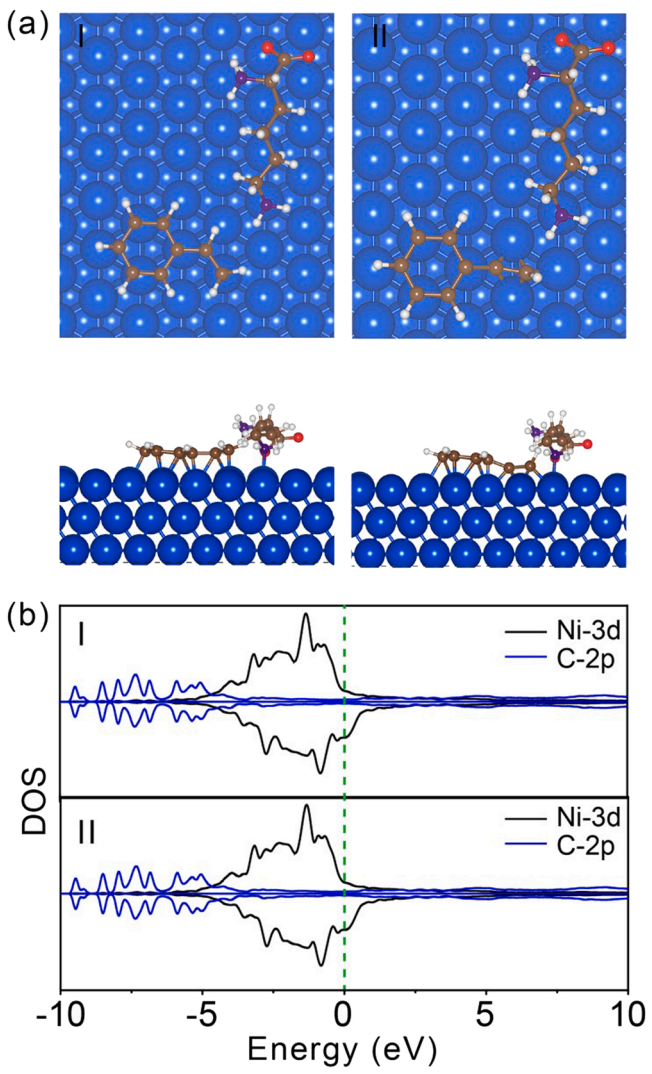

Fig. 5. Adsorption of styrene and phenylacetylene near the $-NH_2$ group on the surface of L-lysine modified Ni(111). (a) Top and side views of the optimized structures with styrene (I) and phenylacetylene (II) adsorbed on the L-1 surface, (b) as well as the corresponding partial density of states (PDOSs).

The reaction containing styrene is also conducted over Ni/Nb_2O_5 to study the effect of charge density of metallic Ni modulated by styrene on the phenylacetylene hydrogenation reaction, (Fig. S17). It can be clearly found that with the increase of styrene content, the phenylacetylene conversion increases firstly and then decreases. According to previous reports [9,44], the increased electron density of metallic Ni is more favorable for the activation of H_2 under visible light irradiation, because high electrons density can provide more opportunities to denote *d*-electrons of Ni NPs to the antibonding orbital of H_2 to accelerate homolytic dissociation of H_2. These results suggest that the electrons state of metallic Ni can be modulated by styrene to increase phenylacetylene conversion. This finding provides an novel understanding for the promoted photocatalytic performance of LSPR metal catalysts through *in situ* electronic state modulation.

Based on the above analysis, a plausable mechanism of phenylacetylene hydrogenation on the surface of Ni/Nb_2O_5 modified with L-lysine molecules is proposed. Firstly, the visible light penetrates L-lysine molecules and the hot electrons generated from metal Ni via LSPR effect can make H_2 to be activated and split into Ni−H [54]. Then phenylacetylene adsorbed on the surface of metallic Ni is transformed into styrene by the hydrogenation process. The productive styrene molecules can increase the charge density on the surface of metal Ni, leading to generate more hot electrons to participate in the activation of H_2, thereby enhancing the conversion of phenylacetylene to styrene. Because styrene has longer distance and smaller adsorption energy on the surface of L-lysine modified metallic Ni than that of phenylacetylene, thereby hindering the excessive hydrogenation of styrene, and finally maintaining the high selectivity of styrene.

3.5. *Extension of L-lysine modification strategy*

The extensional applications of other aromatic alkynes, different supports, different metals and other amino acids modification are summarized in Tables S3-S5. The conversion of aromatic alkynes with electron withdrawing groups (−F and −Cl) is much higher than that with electron donating groups ($-CH_3$ and $-NH_2$) in Table S3. There is no exception that more than 90% of aromatic alkenes selectivity for the aromatic alkynes hydrogenation is achieved over L-$lysine_{0.05}/Ni/Nb_2O_5$ whether the reaction is conducted with or without light irradiation. These results demonstrate that the aromatic alkynes hydrogenation reactions over L-lysine/Ni/Nb_2O_5 have excellent universality.

L-lysine modification strategy is also applicable on different supports, L-$lysine_{0.05}/Ni/Nb_2O_5$ and L-$lysine_{0.05}/Ni/Al_2O_3$ are prepared by the identical impregnation method and subsequent thermal reduction in H_2. It is obvious that the main product over these catalysts without L-lysine modification is ethylbenzene (Table S4, entries 1–3). The selectivity of styrene can reach around 90% over Ni-based catalysts modulated by L-lysine under light. The L-lysine modification strategy has also been applied to other metals including Pt and Pd for hydrogenation of phenylacetylene. It can be clearly seen that this modification strategy does not regulate the selectivity of styrene (Table S4, entries 4 and 5). And compared with the classical Lindlar catalyst, the conversion of phenylacetylene and the selectivity of styrene have been significantly improved (Table S4, entries 1 and 6). These results suggest that L-lysine modification is an effective strategy for Ni-based catalyst in selective phenylacetylene hydrogenation reaction.

Ni/Nb_2O_5 regulated by D-lysine and DL-lysine are also prepared for phenylacetylene hydrogenation (Table S5, entries 1–3). It can be clearly found that L-lysine, D-lysine and DL-lysine can all regulate the selectivity of styrene to more than 90%. Meanwhile, other amino acids are also used to verify whether the selectivity of styrene can be adjusted under visible light irradiation (Table S5, entries 4–6). It can be clearly found that glutamylamine, glutamic acid, and leucine modification can also maintain the selectivity of styrene (around 90%). The results confirm that the photocatalytic activity is not affected by the chirality of lysine, and Ni/Nb_2O_5, modified by amino acids with amino and carboxyl groups at ends is beneficial to improve the selectivity of styrene under light irradiation.

4. Conclusions

L-lysine modified Ni/Nb_2O_5 has been prepared successfully and show excellent photocatalytic performance in the selective hydrogenation of phenylacetylene. Metallic Ni is demonstrated to be the active center for phenylacetylene hydrogenation to styrene under visible light irradiation. And there exist strong interaction between both $-COO^-$ and $-NH_2$ groups of L-lysine and Ni/Nb_2O_5 due to N and O coordination, demonstrated by FT-IR, XPS and DFT calculation, leading to high stability of metallic Ni and L-lysine/Ni/Nb_2O_5. High styrene selectivity is because that the styrene has longer distance and lower adsorption energy on the surface of metallic Ni sites than that of phenylacetylene. The enhanced photocatalytic activity of L-lysine/Ni/Nb_2O_5 is mainly attributed to electrons transfer excited by the LSPR effect of Ni NPs under light irradiation and the enriched electrons on the surface of Ni modulated by styrene *in situ*. This L-lysine modification strategy is also suitable for other Ni-based catalysts. In addition, Ni/Nb_2O_5 modified by other amino acids can also increase the selectivity of styrene. This will provide a prospective protocol to increase olefin selectivity in alkyne

hydrogenation reaction.

CRediT authorship contribution statement

Jie Wang: Conceptualization, Methodology, Formal analysis, Investigation, Data curation, Writing – original draft. **Mengxia Wang**: Formal analysis, Theoretical calculation. **Xincheng Li**: Data curation, Formal analysis. **Xianmo Gu**: Formal analysis, Investigation. **Peng Kong**: Formal analysis. **Ruiyi Wang**: Conceptualization, Supervision, Funding acquisition, Validation. **Xuebin Ke**: Supervision, Writing – review & editing. **Guangtao Yu**: Conceptualization, Supervision, Funding acquisition, Writing – review & editing. **Zhanfeng Zheng**: Conceptualization, Supervision, Funding acquisition, Writing – review & editing.

Declaration of Competing Interest

The authors declare that they have no known competing financial interests or personal relationships that could have appeared to influence the work reported in this paper.

Acknowledgment

This work was supported by the National Natural Science Foundation of China (22072176, 21773284, 21703276, and 21673094), the Shanxi Science and Technology Department (20210302123012), the Hundred Talents Program of the Chinese Academy of Sciences and Shanxi Province, and startup fund for high-level talent at Fujian Normal University. We acknowledge the Computing Center of Jilin Province and the High Performance Computing Center (HPCC) of Jilin University for supercomputer time.

Appendix A. Supporting information

Supplementary data associated with this article can be found in the online version at doi:10.1016/j.apcatb.2022.121449.

References

[1] C. Riley, S. Zhou, D. Kunwar, A. De La Riva, E. Peterson, R. Payne, L. Gao, S. Lin, H. Guo, A. Datye, Design of effective catalysts for selective alkyne hydrogenation by doping of ceria with a single-atom promotor, J. Am. Chem. Soc. 140 (2018) 12964–12973.

[2] Y. Cao, H. Zhang, S. Ji, Z. Sui, Z. Jiang, D. Wang, F. Zaera, X. Zhou, X. Duan, Y. Li, Adsorption site regulation to guide atomic design of Ni-Ga catalysts for acetylene semi-hydrogenation, Angew. Chem. Int. Ed. 59 (2020) 11647–11652.

[3] K. Choe, F.B. Zheng, H. Wang, Y. Yuan, W.S. Zhao, G.X. Xue, X.Y. Qiu, M. Ri, X. H. Shi, Y.L. Wang, G.D. Li, Z.Y. Tang, Fast and selective semihydrogenation of alkynes by palladium nanoparticles sandwiched in metal-organic frameworks, Angew. Chem. Int. Ed. 59 (2020) 3650–3657.

[4] P. Ryabchuk, G. Agostini, M.M. Pohl, H. Lund, A. Agapova, H. Junge, K. Junge, M. Beller, Intermetallic nickel silicide nanocatalyst-A non-noble metal-based general hydrogenation catalyst, Sc. Adv. 4 (2018), eaat0761.

[5] Y.L. Wang, Z.D. Huang, Z. Huang, Catalyst as colour indicator for endpoint detection to enable selective alkyne trans-hydrogenation with ethanol, Nat. Catal. 2 (2019) 529–536.

[6] J. Bu, Z.P. Liu, W.X. Ma, L. Zhang, T. Wang, H.P. Zhang, Q.Y. Zhang, X.L. Feng, J. Zhang, Selective electrocatalytic semihydrogenation of acetylene impurities for the production of polymer-grade ethylene, Nat. Catal. 4 (2021) 557–564.

[7] S. Zhou, L. Shang, Y. Zhao, R. Shi, G.I.N. Waterhouse, Y.C. Huang, L. Zheng, T. Zhang, Pd single-atom catalysts on nitrogen-doped graphene for the highly selective photothermal hydrogenation of acetylene to ethylene, Adv. Mater. 31 (2019) 1900509.

[8] S.Y. Liu, Y.M. Niu, Y.Z. Wang, J.N. Chen, X.P. Quan, X. Zhang, B.S. Zhang, Unravelling the role of active-site isolation in reactivity and reaction pathway control for acetylene hydrogenation, Chem. Commun. 56 (2020) 6372–6375.

[9] L. Zhang, M. Zhou, A. Wang, T. Zhang, Selective hydrogenation over supported metal catalysts: From nanoparticles to single atoms, Chem. Rev. 120 (2020) 683–733.

[10] Z. Wei, Z. Yao, Q. Zhou, G. Zhuang, X. Zhong, S. Deng, X. Li, J. Wang, Optimizing alkyne hydrogenation performance of Pd on carbon in situ decorated with oxygen-deficient TiO_2 by integrating the reaction and diffusion, ACS Catal. 9 (2019) 10656–10667.

[11] H. Liang, B. Zhang, H. Ge, X. Gu, S. Zhang, Y. Qin, Porous TiO_2/Pt/TiO_2 sandwich catalyst for highly selective semihydrogenation of alkyne to olefin, ACS Catal. 7 (2017) 6567–6572.

[12] B. Bridier, J. Perez-Ramirez, Cooperative effects in ternary Cu-Ni-Fe catalysts lead to enhanced alkene selectivity in alkyne hydrogenation, J. Am. Chem. Soc. 132 (2010) 4321–4327.

[13] E.V. Golubina, E.S. Lokteva, A.V. Erokhin, A.A. Veligzhanin, Y.V. Zubavichus, V. A. Likholobov, V.V. Lunin, The role of metal–support interaction in catalytic activity of nanodiamond-supported nickel in selective phenylacetylene hydrogenation, J. Catal. 344 (2016) 90–99.

[14] N. Carrara, C. Betti, F. Coloma-Pascual, M.C. Almansa, L. Gutierrez, C. Miranda, M. E. Quiroga, C.R. Lederhos, High-active metallic-activated carbon catalysts for selective hydrogenation, Int. J. Chem. Eng. 2018 (2018) 1–11.

[15] Y. Liu, J. Zhao, J. Feng, Y. He, Y. Du, D. Li, Layered double hydroxide-derived Ni-Cu nanoalloy catalysts for semi-hydrogenation of alkynes: Improvement of selectivity and anti-coking ability via alloying of Ni and Cu, J. Catal. 359 (2018) 251–260.

[16] J.W. Yu, X.Y. Wang, C.Y. Yuan, W.Z. Li, Y.H. Wang, Y.W. Zhang, Synthesis of ultrathin Ni nanosheets for semihydrogenation of phenylacetylene to styrene under mild conditions, Nanoscale 10 (2018) 6936–6944.

[17] Y. Long, J. Li, L. Wu, Q. Wang, Y. Liu, X. Wang, S. Song, H. Zhang, Construction of trace silver modified core@shell structured Pt-Ni nanoframe@CeO_2 for semihydrogenation of phenylacetylene, Nano Res. 12 (2019) 869–875.

[18] K. Murugesan, C.B. Bheeter, P.R. Linnebank, A. Spannenberg, J.N.H. Reek, R. V. Jagadeesh, M. Beller, Nickel-catalyzed stereodivergent synthesis of *E*- and *Z*-Alkenes by hydrogenation of alkynes, ChemSusChem 12 (2019) 3363–3369.

[19] P.C. Rath, M. Mishra, D. Saikia, J.K. Chang, T.-P. Perng, H.-M. Kao, Facile fabrication of titania-ordered cubic mesoporous carbon composite: Effect of Ni doping on photocatalytic hydrogen generation, Int. J. Hydrog. Energ. 44 (2019) 19255–19266.

[20] C. Li, Y. Chen, S. Zhang, J. Zhou, F. Wang, S. He, M. Wei, D.G. Evans, X. Duan, Nickel-gallium intermetallic nanocrystal catalysts in the semihydrogenation of phenylacetylene, ChemCatChem 6 (2014) 824–831.

[21] Y. Cao, H. Zhang, S. Ji, Z. Sui, Z. Jiang, D. Wang, F. Zaera, X. Zhou, X. Duan, Y. Li, Adsorption site regulation to guide atomic design of Ni-Ga catalysts for acetylene semi-hydrogenation, Angew. Chem. Int. Ed. 59 (2020) 11647–11652.

[22] L. Yang, S. Yu, C. Peng, X. Fang, Z. Cheng, Z. Zhou, Semihydrogenation of phenylacetylene over nonprecious Ni-based catalysts supported on AlSBA-15, J. Catal. 370 (2019) 310–320.

[23] Y. Niu, X. Huang, Y. Wang, M. Xu, J. Chen, S. Xu, M.G. Willinger, W. Zhang, M. Wei, B. Zhang, Manipulating interstitial carbon atoms in the nickel octahedral site for highly efficient hydrogenation of alkyne, Nat. Commun. 11 (2020) 3324.

[24] X. Shi, X. Wen, S. Nie, J. Dong, J. Li, Y. Shi, H. Zhang, G. Bai, Fabrication of Ni_3N nanorods anchored on N-doped carbon for selective semi-hydrogenation of alkynes, J. Catal. 382 (2020) 22–30.

[25] S.G. Kwon, G. Krylova, A. Sumer, M.M. Schwartz, E.E. Bunel, C.L. Marshall, S. Chattopadhyay, B. Lee, J. Jellinek, E.V. Shevchenko, Capping ligands as selectivity switchers in hydrogenation reactions, Nano Lett. 12 (2012) 5382–5388.

[26] A.M. López-Vinasco, L.M. Martínez-Prieto, J.M. Asensio, P. Lecante, B. Chaudret, J. Cámpora, P.W.N.M. van Leeuwen, Novel nickel nanoparticles stabilized by imidazolium-amidinate ligands for selective hydrogenation of alkynes, Catal. Sci. Technol. 10 (2020) 342–350.

[27] R.K. Rai, M.K. Awasthi, V.K. Singh, S.R. Barman, S. Behrens, S.K. Singh, Aqueous phase semihydrogenation of alkynes over Ni–Fe bimetallic catalysts, Catal. Sci. Technol. 10 (2020) 4968–4980.

[28] D. Mateo, N. Morlanes, P. Maity, G. Shterk, O.F. Mohammed, J. Gascon, Efficient visible-light driven photothermal conversion of CO_2 to methane by nickel nanoparticles supported on barium titanate, Adv. Funct. Mater. (2020) 2008244.

[29] H. Liu, T.D. Dao, L. Liu, X. Meng, T. Nagao, J. Ye, Light assisted CO_2 reduction with methane over group VIII metals: Universality of metal localized surface plasmon resonance in reactant activation, Appl. Catal., B 209 (2017) 183–189.

[30] Y. Zhang, L. Pei, Z. Zheng, Y. Yuan, T. Xie, J. Yang, S. Chen, J. Wang, E. R. Waclawik, H. Zhu, Heterojunctions between amorphous and crystalline niobium oxide with enhanced photoactivity for selective aerobic oxidation of benzylamine to imine under visible light, J. Mater. Chem. A 3 (2015) 18045–18052.

[31] H.Y. Zhu, Z.F. Zheng, X.P. Gao, Y.N. Huang, Z.M. Yan, J. Zou, H.M. Yin, Q.D. Zou, S.H. Kable, J.C. Zhao, Y.F. Xi, W.N. Martens, R.L. Frost, Structural evolution in a hydrothermal reaction between Nb_2O_5 and NaOH solution: From Nb_2O_5 grains to microporous $Na_2Nb_2O_6.2/3H_2O$ fibers and $NaNbO_3$ cubes, J. Am. Chem. Soc. 128 (2006) 2373–2384.

[32] J. Wang, X. Gu, L. Pei, P. Kong, J. Zhang, X. Wang, R. Wang, E.R. Waclawik, Z. Zheng, Strong metal-support interaction induced O_2 activation over Au/MNb_2O_6 (M = Zn^{2+}, Ni^{2+} and Co^{2+}) for efficient photocatalytic benzyl alcohol oxidative esterification, Appl. Catal., B 283 (2021), 119618.

[33] A.D. Becke, A new mixing of Hartree-Fock and local density-functional theories, J. Chem. Phys. 98 (1993) 1372–1377.

[34] G. Kresse, J. Hafner, Ab initio molecular dynamics for liquid metals, Phys. Rev. B 47 (1993) 558–561.

[35] G. Kresse, J. Hafner, Ab initio molecular-dynamics simulation of the liquid-metal–amorphous-semiconductor transition in germanium, Phys. Rev. B 49 (1994) 14251–14269.

[36] X. Wu, M.C. Vargas, S. Nayak, V. Lotrich, G. Scoles, Towards extending the applicability of density functional theory to weakly bound systems, J. Chem. Phys. 115 (2001) 8748–8757.

[37] P.E. Blöchl, Projector augmented-wave method, Phys. Rev. B 50 (1994) 17953–17979.

[38] G. Kresse, D. Joubert, From ultrasoft pseudopotentials to the projector augmented-wave method, Phys. Rev. B 59 (1999) 1758–1775.
[39] K. Ramya, N.T. Saraswathi, C.R. Raja, Growth and characterization of L-Lysine adipate crystal, Opt. Laser Technol. 90 (2017) 222–225.
[40] K.E. Wilson, C.J. Baddeley, Chiral assemblies of nickel lysinate via the corrosive adsorption of (S)-lysine on Ni/Au{111}, Surf. Sci. 629 (2014) 102–107.
[41] V. Humblot, C. Methivier, C.M. Pradier, Adsorption of L-lysine on Cu(110): A RAIRS study from UHV to the liquid phase, Langmuir 22 (2006) 3089–3096.
[42] D. Mateo, J. Albero, H. García, Graphene supported NiO/Ni nanoparticles as efficient photocatalyst for gas phase CO_2 reduction with hydrogen, Appl. Catal., B 224 (2018) 563–571.
[43] S. Li, L. Wang, Y. Li, L. Zhang, A. Wang, N. Xiao, Y. Gao, N. Li, W. Song, L. Ge, J. Liu, Novel photocatalyst incorporating Ni-Co layered double hydroxides with P-doped CdS for enhancing photocatalytic activity towards hydrogen evolution, Appl. Catal., B 254 (2019) 145–155.
[44] J. Ni, W. Leng, J. Mao, J. Wang, J. Lin, D. Jiang, X. Li, Tuning electron density of metal nickel by support defects in Ni/ZrO_2 for selective hydrogenation of fatty acids to alkanes and alcohols, Appl. Catal., B 253 (2019) 170–178.
[45] Y. Yang, X. Sun, G. Han, X. Liu, X. Zhang, Y. Sun, M. Zhang, Z. Cao, Y. Sun, Enhanced electrocatalytic hydrogen oxidation on Ni/NiO/C derived from a nickel-based metal-organic framework, Angew. Chem. Int. Ed. 58 (2019) 10644–10649.
[46] J. Xu, T. White, P. Li, C.H. He, J.G. Yu, W.K. Yuan, Y.F. Han, Biphasic Pd-Au Alloy Catalyst for Low-Temperature CO Oxidation, J. Am. Chem. Soc. 132 (2010) 10398–10406.
[47] N. Merlin, B.A. Nogueira, V.A. de Lima, L.M. dos Santos, Application of Fourier transform infrared spectroscopy, chemical and chemometrics analyses to the characterization of agro-industrial waste, Quim. Nova 37 (2014) 1584–1588.
[48] X.Y. Wang, R.Y. Wang, X.M. Gu, J.F. Jia, Z.F. Zheng, Light-assisted O-methylation of phenol with dimethyl carbonate over a layered double oxide catalyst, Catal. Sci. Technol. 9 (2019) 1774–1778.
[49] X. Zhang, X. Ke, H. Zhu, Zeolite-supported gold nanoparticles for selective photooxidation of aromatic alcohols under visible-light irradiation, Chem. Eur. J. 18 (2012) 8048–8056.
[50] S. Sarina, E.R. Waclawik, H. Zhu, Photocatalysis on supported gold and silver nanoparticles under ultraviolet and visible light irradiation, Green. Chem. 15 (2013) 1814–1833.
[51] Q. Xiao, S. Sarina, E. Jaatinen, J.F. Jia, D.P. Arnold, H.W. Liu, H.Y. Zhu, Efficient photocatalytic Suzuki cross-coupling reactions on Au-Pd alloy nanoparticles under visible light irradiation, Green. Chem. 16 (2014) 4272–4285.
[52] Q. Xiao, Z. Liu, A. Bo, S. Zavahir, S. Sarina, S. Bottle, J.D. Riches, H. Zhu, Catalytic transformation of aliphatic alcohols to corresponding esters in O_2 under neutral conditions using visible-light irradiation, J. Am. Chem. Soc. 137 (2015) 1956–1966.
[53] Z. Xiong, X. Chen, X. Wang, L. Peng, D. Yan, H. Lei, Y. Fu, J. Wu, Z. Li, X. An, W. Wu, Size dependence of plasmon absorption of Ni nanoparticles embedded in $BaTiO_3/SrTiO_3$ superlattices, Appl. Surf. Sci. 268 (2013) 524–528.
[54] A. Solis-Garcia, J.F. Louvier-Hernandez, A. Almendarez-Camarillo, J.C. Fierro-Gonzalez, Participation of surface bicarbonate, formate and methoxy species in the carbon dioxide methanation catalyzed by ZrO_2-supported Ni, Appl. Catal., B 218 (2017) 611–620.